Gradient Hydrogel Matrix for Microarray and Biosensor Applications: An Imaging SPR Study

Olof Andersson, Andréas Larsson, Tobias Ekblad, and Bo Liedberg*

Division of Sensor Science and Molecular Physics, Department of Physics, Chemistry and Biology, Linköping University, SE-581 83 Linköping, Sweden

Received September 14, 2008; Revised Manuscript Received November 11, 2008

A biosensor matrix based on UV-initiated graft copolymerized poly(ethylene glycol) methacrylate and 2-hydroxyethyl methacrylate has been studied using imaging surface plasmon resonance (iSPR). By using a photo mask and a programmable shutter to vary the exposure time laterally, a gradient of matrix spots with physical thicknesses ranging from a few to tens of nanometers was generated. To maximize the dynamic range, imaging SPR was employed in wavelength interrogation mode. By finding the minimum in the reflectance spectra from each pixel of an image, SPR wavelength maps were constructed. The shift in SPR wavelength upon biospecific interaction was then measured both as a function of matrix thickness and composition. The performance of the matrix was evaluated in terms of immobilization of human serum albumin, biomolecular interaction with its antibody, and nonspecific binding of human fibrinogen. In addition, a low molecular weight interaction pair based on a synthetic polypeptide and calmodulin was also studied to explore the size selectivity of the hydrogel matrix. Our results show that the gradient matrix exhibits excellent properties for quick evaluation and screening of optimal hydrogel performance. The mixed hydrogel matrices display very low levels of nonspecific binding. It is also evident that the low molecular weight calmodulin is capable of freely diffusing and interacting throughout the entire hydrogel matrix, whereas the much larger albumin and its corresponding antibody, in particular, are partly/completely hindered from penetrating the interior of the matrix. This size-selectivity is attributed to a significant UV-initiated cross-linking or branching of the matrix during fabrication and/or protein mediated multipoint attachment during immobilization.

Introduction

The use of surface enhancing matrices, for instance hydrogels, is of great interest for the development of efficient and robust biosensors. Well-designed biosensor matrices exhibit low nonspecific binding while allowing for covalent immobilization of ligands with maintained biofunctionality and minimal leaching. The carboxymethylated dextran matrix is an example of a hydrogel that has been extensively used in biointeraction analysis.[1] Other approaches include sol−gel encapsulation[2,3] and hydrogel matrices based on different forms of poly(ethylene glycol) (PEG).[4−8] In earlier work, we have developed such a matrix, based on graft copolymerization of PEG methacrylate and 2-hydroxyethyl methacrylate (HEMA) monomers.[9−11] In protein microarray applications, for example, it is crucial to be able to immobilize different proteins to separate regions on the same sensor chip without cross-contamination between neighboring spots. On homogeneous dextran hydrogel surfaces, this has been accomplished through introduction of reversible hydrophobic barriers in a grid-like pattern.[12,13] A two-dimensional micro array platform based on self-assembled monolayers (SAMs) of oligo(ethylene glycol) (OEG)-containing alkanethiols was recently developed by Valiokas et al.[14] In this case, a hydrophobic grid consisting of microcontact printed alkanethiols, later passivated with bovine serum albumin, was used to prevent cross-contamination between neighboring OEG-spots. Kannan et al.[15] used photolithographic techniques to create passive barriers of PEG between functional regions on a micro array chip.

In the present work, a biosensor polymer matrix composed of PEG methacrylate with an average EG chain length of 10 units ($PEG_{10}MA$) and HEMA was graft polymerized using UV-initiated free radical copolymerization. By using a photo mask, an array of circular spots, 200 μm in diameter, was exposed to UV light (254 nm). The use of a programmable shutter enabled us to vary the exposure time of adjacent spots in the matrix. In this way, rows of spots with thicknesses ranging from 1−50 nm were produced on the same chip.[9,11] As substrate for grafting of the polymer matrix, a SAM of methoxyl-terminated OEG thiols on glass surfaces coated with a thin layer of gold was used. The resulting array consisted of circular spots of hydrogel matrix with varying thicknesses surrounded by a monolayer of OEG thiols. As will be shown, the OEG thiol layer was completely passive in terms of nonspecific adsorption. Monitoring of biomolecular binding events to surfaces incorporating numerous spots in an array format requires imaging techniques with high lateral resolution or capabilities of scanning the surface. One such method is surface plasmon resonance (SPR), an established optical sensor technique first introduced in biosensor context in the 1980s[16] and which is now commonly employed in biomolecular interaction analysis (BIA). SPR is a very surface sensitive technique based on measuring changes in the optical properties in the vicinity of the sensor surface.[17,18] A major quality of SPR is the possibility to perform measurements in situ in a complex liquid ambient. By using an imaging detector, SPR can be extended to provide measurements with lateral resolution.[19] Typically, the measured quantity in SPR sensors is the shift in resonance angle ($\Delta\theta_{SPR}$) upon binding of biomolecules and this shift is proportional to the surface concentration of bound molecules.[20] In an imaging SPR (iSPR)

* To whom correspondence should be addressed. Phone: +46-13-28 16 89. E-mail: bolie@ifm.liu.se.

10.1021/bm801029b CCC: $40.75
Published on Web 12/09/2008

setup, the angle of incidence is usually fixed and the measured parameter is the change in intensity as the resonance angle shifts. In this case, the dynamic range is limited by the half-width of the SPR curve. To extend the dynamic range, the angle of incidence can be scanned over an interval to find θ_{SPR} of each pixel in the image. Angular scanning, however, can be a disadvantage in an imaging setup because the oblique angle will cause the magnification to be different as the angle of incidence is varied. In 1988, Zhang et al. introduced an SPR sensor based on measurement of the resonance wavelength (λ_{SPR}) at a fixed angle of incidence.[21] More recently, Yuk et al. employed spectral interrogation imaging SPR to study antigen−antibody interactions in an array format.[22,23] The sensitivity of SPR sensors in different variations based on $\Delta\lambda_{SPR}$ measurements has been thoroughly investigated by Homola[24] and Yuk et al.[25,26] Because of the large difference in thickness of the spots on our sensor surface, a large dynamic range needs to be covered during characterization. Therefore, in this study, we have used spectral iSPR to study, in situ, immobilization and biointeractions within our hydrogel matrix spot gradient. As model systems, we have used the covalent immobilization of human serum albumin (HSA) to the hydrogel matrix and its interaction with anti-HSA and the interaction between an immobilized synthetic polypeptide and calmodulin. Furthermore, the composition of the matrix spots was varied by changing the $PEG_{10}MA$/HEMA ratio in the monomer solution. In addition to $\Delta\lambda_{SPR}$ measurements, imaging ellipsometry was used to measure the thickness of the graft polymerized matrix spots. This type of surfaces, with spots of varying thicknesses and differently composed surface chemistries can be used in optimization of matrices for biosensor applications. Spots of different thicknesses accommodated on the same chip can be useful in protein micro arraying, particularly when there are large variations in the molecular sizes of the analytes or when the affinities of the ligands are very different. In particular, thick hydrogel matrix spots with large immobilization capacity are good for small molecular and low affinity interactions, whereas thinner spots with a lower capacity are more suitable for large molecules and high affinity ligands. By using an imaging technique, such as iSPR, and in situ measurements, screening for optimal biosensor performance can be made easier.

Materials and Methods

Chip Manufacture. Before use, glass slides (12 × 12 mm^2) coated with a thin layer of gold (45 nm) were cleaned in a mixture of Milli-Q water (Milli-Q, Millipore), 30% hydrogen peroxide (Merck KGaA, Germany), and 25% ammonia (Merck KGaA) for 10 min at 85 °C. The surfaces were provided by Biacore (part of GE Healthcare). After cleaning the gold surfaces, they were immersed in a solution of $HS(CH_2)_{11}CONH(C_2H_4O)_{11}CH_3$ (Polypure AS, Norway) with a concentration of 100 μM in 99.5% ethanol for a minimum of 24 h at room temperature, forming oligo(ethylene glycol) monolayers (OEG-SAM). After incubation, the surfaces were rinsed in 99.5% ethanol and ultrasonicated for 3 min before being dried under a nitrogen flow. In earlier work, the process of grafting the hydrogel matrix onto cycloolefin polymer substrates[10] and onto SAMs on gold surfaces[11] has been extensively described. In brief, a chromium-coated quartz wafer was photolithographically patterned with circular spots of 200 μm in diameter and used as a photo mask. A small drop of a mixture of the monomers was applied to the quartz mask from beneath and brought in contact with the SAM-coated gold surface. The surface tension held the substrate in place under the mask. A movable shutter was visually aligned to the pattern of the photo mask, and the UV exposure time was varied by moving the motorized shutter. The shutter was moved in steps of 300 μm every 20 s for a total of 5 min. The entire grafting setup was enclosed in an airtight chamber which was purged with nitrogen gas for one minute before and throughout the grafting process. The lightsource used for the grafting was a Philips TUV PL-L 18W Hg lamp with a sharp emission peak at 254 nm. In this work, we have used the monomers $PEG_{10}MA$ and HEMA (both from Sigma-Aldrich, Sweden AB) dissolved in Milli-Q water to a total concentration of 240 mM in mixtures with HEMA content 25, 50, 75, and 100%, respectively. Following graft polymerization, carboxyl groups were introduced in the hydrogel matrix by treatment with bromoacetic acid.[1] The carboxylated hydrogel substrates were stored immersed in Milli-Q water at 4 °C until further use.

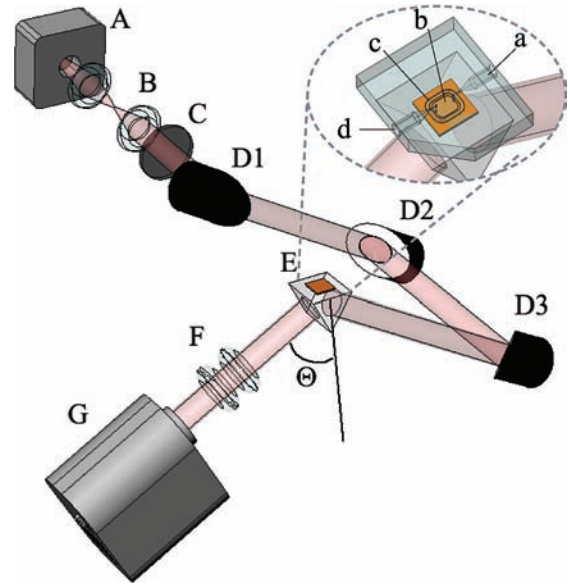

Figure 1. Schematic view of the imaging SPR instrument consisting of monochromator (A), collimating optics (B), rotatable polarizer (C), mirrors (D1-D3), prism and sensor surface (E), imaging optics (F), and CCD detector (G). The inset shows a magnification of the prism and sensor surface with the PMMA flow system docked: inlet (a), flow cell (b), O-ring casket (c), and outlet (d). The angle of incidence, θ, can be adjusted between 40−84° by simultaneously rotating the mirrors and the detector.

Imaging Ellipsometry. An imaging null ellipsometer (EP^3, Nanofilm Technologie, Germany) was used to measure the thickness of the graft polymerized hydrogel. The ellipsometer was operated at a wavelength of 831 nm, with the angle of incidence set at 60°. In the imaging ellipsometer experiments, surfaces were treated in the same way as described above, but the gold thickness of the substrates was 200 nm. The refractive index of the organic material on the surface was assumed to be 1.5.

Imaging Surface Plasmon Resonance. The iSPR measurements were performed using an in-house custom built instrument based on spectral interrogation (Figure 1). The iSPR instrument was comprised of two angular rotation stages (RV160, Newport Inc.) with synchronously movable arms, enabling a choice of incidence and reflection angles ranging from 40−84°. Surface plasmons were excited by means of a 25 mm equilateral prism (BK7 glass, Melles Griot Inc.), a so-called attenuated total reflection (ATR) coupler. A refractive index matching gel (Cargille Inc.) was used to achieve optical contact between the prism and the substrate surfaces. Light from a monochromator (SpectraPro 300i, Acton Research Corp.) was collimated and TM-polarized before being guided toward the prism by means of mirrors mounted on one of the movable arms. The grating density was 300 mm^{-1} and the wavelength interval used in this work was 600−800 nm. A CCD detector (Retiga Exi, Qimaging Corp., 12 bit 1 MP without IR filter) with imaging optics was mounted on the opposite movable arm. The camera was connected to a computer through an IEEE-1394 interface and custom software designed within the National Instruments LabVIEW environment was used to acquire and save image data. The

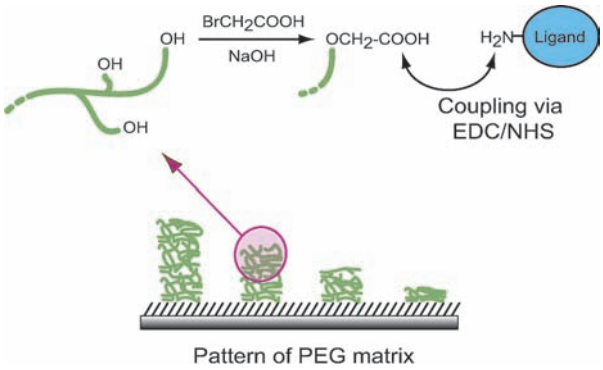

Figure 2. Covalent coupling of biomolecules to the hydrogel matrix. The -OH groups in the polymer are carboxylated using bromoacetic acid. Reactive esters are then introduced using EDC/NHS. Immobilization occurs via primary amines on the ligand.

same software was used to control the monochromator and motorized arms via an IEEE-488 interface. During the iSPR measurements the angle of incidence was kept fixed at 72.5°. At this angle, one pixel on the CCD detector corresponded to an area of 2.2 × 8.2 μm^2 on the sample surface. The wavelength was scanned at a speed of 100 nm/min. A flow cell milled from PMMA with physical dimensions of 5 × 5 × 0.1 mm^3 was used to inject samples over the SPR substrates. The PMMA cell was sealed to the surface with a nitril rubber O-ring. A syringe pump was used to keep a constant flow of buffer at a rate of 30 μL/min. Wavelength scans were acquired before and after injections of samples with the flow system. During the wavelength scans, images were saved at a rate of ~0.6 Hz. Raw data from a complete wavelength scan comprised an image-stack of reflectivity data. Typically, 121 images in the stack constituted a full scan over a range of 200 nm. The output from the monochromator varied with wavelength, as did the sensitivity of the CCD camera. Normalization was achieved by turning the polarizer 90° and making a scan of the reflection of TE-polarized light. After a complete wavelength scan, the reflection spectrum of each pixel was interpolated to be equidistant and thereafter divided by the corresponding pixels spectrum from reflection of TE-polarized light. The wavelength giving a minimum in reflection, the SPR wavelength (λ_{SPR}) was found by using a weighted centroid algorithm.[27] To reduce noise, only the pixels with a reflectivity below 40% were used in the calculation of the SPR wavelength. The result of a weighted centroid calculation of the image stack will be referred to as an SPR map throughout this work. In addition to a full SPR map, SPR curves from selected regions of interest could also be acquired.

Biomolecular Interaction Analysis: HSA and HFib. During the biomolecular interaction analysis, hepes-buffered saline pH 7.4 (HBS-EP, GE Healthcare) also containing 0.005% surfactant Tween P20 was used as running buffer. The carboxylated hydrogel surfaces were activated through a 5 min long injection of an aqueous mixture of 0.05 M *N*-hydroxysuccinimide (NHS) and 0.2 M *N*-ethyl-*N*′-[3-(dimethylamino)-propyl]carbodiimide (EDC; Figure 2). After immobilization, the hydrogel was deactivated through a 7 min long injection of ethanolamine (1 M). Both the EDC/NHS and the ethanolamine were provided by GE Healthcare. Human serum albumin (HSA) was purchased from Sigma-Aldrich and dissolved to a concentration of 700 nM (50 μg/mL) in 10 mM sodium acetate buffer, pH 4.5 (GE Healthcare). Polyclonal rabbit anti-HSA (aHSA) was purchased from Dakocytomation A/S, Denmark, and dissolved in HBS-EP to a concentration of 300 nM (50 μg/mL). The contact time for all injections of HSA and aHSA was 5 min. The nonspecific binding of human fibrinogen (HFib; Hyphen BioMed SAS) to the hydrogel matrices was studied through a 5 min long injection of HFib dissolved in HBS-EP to a concentration of 1.4 μM (500 μg/mL).

Biomolecular Interaction Analysis: Calmodulin. Calmodulin (CaM) and the calmodulin binding domain (CBD), a 20-mer fragment of myosin light chain kinase were purchased from Calbiochem. The molecular weight of CaM is 17 kDa and of the CBD-peptide 2.3 kDa.

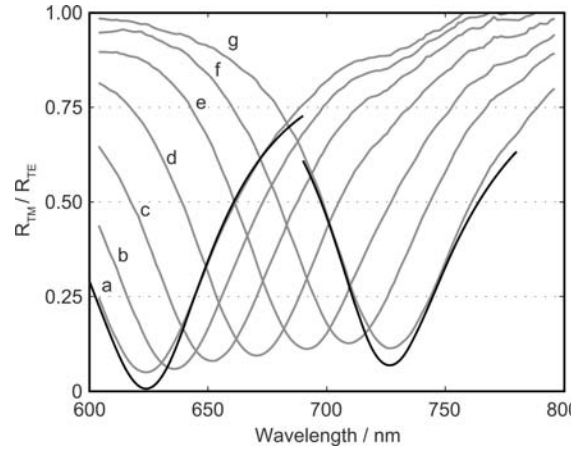

Figure 3. Measured (gray) and calculated (black) SPR reflectivity curves from hydrogel spots of different thicknesses. The curves were normalized by taking the quota between reflection of TM-polarized and TE-polarized light. As the UV grafting time increases, in steps of 20 s, from 120 s (curve a) to 240 s (curve g), the resulting thickness of the hydrogel spots becomes higher and λ_{SPR} shifts to longer wavelengths.

Calmodulin was reconstituted and diluted to the desired concentrations (0.3−100 μg/mL) in HBS-N (hepes buffer without EDTA or surfactant), with an addition of 6 mM $CaCl_2$ (Merck). The CBD-peptide was dissolved to a concentration of 90 μM (200 μg/mL) in 10 mM K/Na-phosphate, pH 6.8. The CBD peptide was immobilized to the hydrogel spot gradient surface by activation using EDC/NHS for 6 min, followed by an injection of CBD for 7 min. Ethanolamine was then injected for 6 min to deactivate any remaining unreacted esters. The response upon introduction of calmodulin in the presence of calcium was then measured two minutes into the CaM injections.

Results and Discussion

Imaging Surface Plasmon Resonance Measurements. Throughout this work, we will use the shift in SPR wavelength ($\Delta\lambda_{SPR}$) as a quantitative measure of the amount of organic material that binds to the hydrogel matrix spot gradient surfaces. The SPR wavelength of a particular region of the sensor surface was determined by making a scan over the wavelength region 600−800 nm and finding the wavelength that exhibits a minimum in the reflection spectrum. Figure 3 shows measured reflectivity curves (gray lines, a−g) from spots of different thicknesses on a surface that was graft polymerized from an equimolar PEG_{10}MA/HEMA mixture. For reference, calculated curves (black lines) for the thinnest and thickest spots are also included. The first calculated curve (λ_{SPR} 620 nm) corresponds to the gold film with only the SAM present. In the second solid curve of Figure 3 (λ_{SPR} 725 nm) the presence of an additional 68 nm thick matrix layer was included in the calculations. The calculations were made using the Fresnel reflection coefficient formulas for a five layer optical system and the equations derived by Hansen.[28] Data for the dielectric constant of the glass substrate was obtained from Schott AG. Refractive index data for the gold layer was measured by spectroscopic ellipsometry. The angle of incidence was 72.5° and the thickness of the underlying HS-UDA-mPEG SAM was 3.1 nm. In these calculations, the refractive index of the hydrogel matrix was assumed to be 1.42 over the entire spectrum (based on spectroscopic ellipsometry measurements in aqueous ambient). It is clear from the measured curves in Figure 3 that λ_{SPR} shifts toward longer wavelengths with increasing matrix thickness. Theoretical expressions for the sensitivity of SPR sensors based on spectral

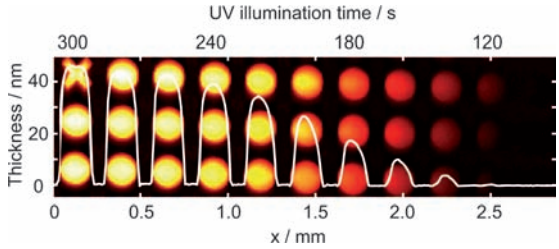

Figure 4. Line profile showing the thickness, determined by ellipsometry, of an UV grafted hydrogel chip with 50% HEMA content. The exposure time was varied in 20 s steps from left to right, where the leftmost spot column was exposed for a total of 300 s. A minimum of 140 s UV-exposure was required for polymer grafting to begin. The background is a thickness map, measured by imaging ellipsometry, showing three rows of the hydrogel spot gradient surface.

interrogation ($\delta\lambda_{SPR}/\delta n$) have been derived by Homola.[24] The sensitivity depends on the dispersion of the prism, the refractive index of the sensing medium and also varies with the wavelength. For a 50 nm gold film on BK7 glass with air as the sensing medium, the sensitivity to changes in the refractive index in the vicinity of the sensor surface is reported to lie at around 8 nm/mRIU at 600 and 11 nm/mRIU at 800 nm. In aqueous media the sensitivity is reduced by a factor of 2.[25] These values are valid under the assumption that the sensing layer extends throughout the SPR probe depth, which typically falls in the range 80−150 nm.[29] In our case, the hydrogel thickness is much smaller than the probe depth. Under these conditions another interesting parameter is the SPR response to changes in the thickness of the hydrogel layer. For example, the sensitivity ($\delta\lambda_{SPR}/\delta d$) has been reported to vary between approximately 11 at $\lambda = 600$ nm and 13 at $\lambda = 700$ nm for a thin film in air.[24] Our calculations, based on the Fresnel formulas and with our experimental setup, show that for addition of a thin film ($d =$ 1 nm) with refractive index $n = 1.45$ on top of our matrix spots, in an aqueous ambient, the SPR wavelength will shift by ~2.0 nm for the thinnest and by ~1.8 nm for the thickest spots. When there is a uniform increase in refractive index of the hydrogel matrix, the SPR wavelength of the thickest spots ($d = 70$ nm) increases by ($\delta\lambda_{SPR}/\delta n$) ≈ 1.4 nm/mRIU. Furthermore, the variation in sensitivity with respect to hydrogel thickness is approximately linear with a slope of ~0.02 $mRIU^{-1}$. Therefore, a quantitative difference in $\Delta\lambda_{SPR}$ between spots of different thickness can be interpreted as signifying more uniform binding throughout the hydrogel, whereas when there is no or little difference between the spots it can be concluded that the molecular species are unable or hindered to penetrate the matrix.

Thickness of the Hydrogel Spot Gradient. Imaging ellipsometry was employed to study the thickness profile of the graft polymerized spot gradient. Figure 4 shows the ellipsometric thickness profile of a hydrogel matrix spot gradient from a monomer solution with a 50% HEMA composition. The spots are 200 μm in diameter with a separation of 100 μm. The thickest (leftmost) spots were graft polymerized for 5 min, resulting in a final thickness of about 45 nm. The first sign of grafting appears after a UV exposure time of 2 min and 20 s, in agreement with previous results for similar patterned surfaces.[9] It is likely that this start-up period is necessitated by the presence of inhibitors and oxygen, which need to be depleted before grafting can begin. Thus, diffusion of these interfering species from the nonilluminated areas into the spot areas is believed to be the reason for the observed lag time. Analogously, this is also considered to be the cause of the inclined appearance of the matrix spots, as seen in Figure 5, which are particularly obvious in the line profiles of Figure 5B. The grafting appears

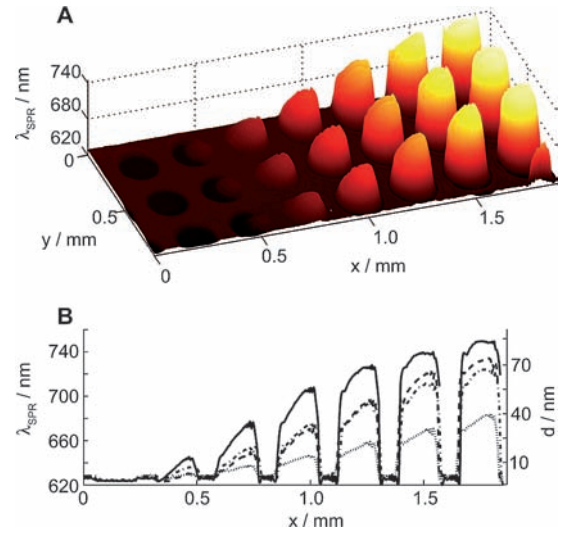

Figure 5. (A) SPR wavelength map of a hydrogel spot gradient surface with a HEMA content of 75%. (B) Line profiles of spot gradients grafted with different HEMA content. From the top down, 25 (solid), 75 (dashed), 50 (dash-dot), and 100% HEMA (dotted). The rightmost axis shows the calculated hydrogel matrix thickness based on a refractive index of $n = 1.42$.

to be more efficient on the side of the spots facing areas that have experienced a longer UV light exposure time than on the side adjacent to areas that have been exposed for a shorter time. After about four minutes of grafting, the thickness starts to level off. The complete gradient consists of eleven spots with distinctly different thicknesses ranging from about 5−45 nm in the dry state. Figure 5A shows an iSPR surface map of a hydrogel matrix spot gradient with a HEMA content of 75%. In the SPR surface map, only the first seven spots of the thickness gradient are shown. Chromatic aberration lowers the resolution and somewhat blurs the features of the hydrogel spots, making accurate calculation of λ_{SPR} at the edges difficult and results in sharp rims surrounding the spots in the SPR map and in the line profiles (visible as spikes in Figure 6C and D). The UV exposure time over the seven spots of the SPR map ranges from 140 to 220 s. This is the region of the gradient studied for the remainder of this paper. The SPR angle varies between about 620 and 740 nm over this region. Figure 5B shows line profiles taken across one gradient row from surfaces graft polymerized with different $PEG_{10}MA$/HEMA mixing ratios. With the exception of 100% HEMA (lower dotted line), the mixing ratio of the monomer solution seems to have only a minor effect on the final thickness of the hydrogel, and the slight variation in slope and thickness of the 25, 50, and 75% HEMA gradients cannot be unambiguously interpreted as an effect of polymer mixture but rather reflects the reproducibility of the grafting method. In earlier work, we have established that the degradation rate of polymerized HEMA, due to UV exposure during grafting, is much greater than that of $PEG_{10}MA$ (which hardly degrades at all), leading to an intrinsically thinner matrix when grafting from 100% HEMA monomer solutions.[10]

Immobilization and Biomolecular Interaction Analysis. The ability of the carboxylated matrix to perform in biospecific interaction analysis was studied by iSPR. As a model system, we used the interaction between HSA (M_w 66 kDa) and aHSA (M_w 146 kDa). Following carboxylation, the spot gradient surfaces were docked into the iSPR instrument and the protein ligand, HSA, was covalently coupled to the matrix using amine-coupling (Figure 2). In Figure 6A, the SPR angle shift upon HSA immobilization to three differently composed hydrogel

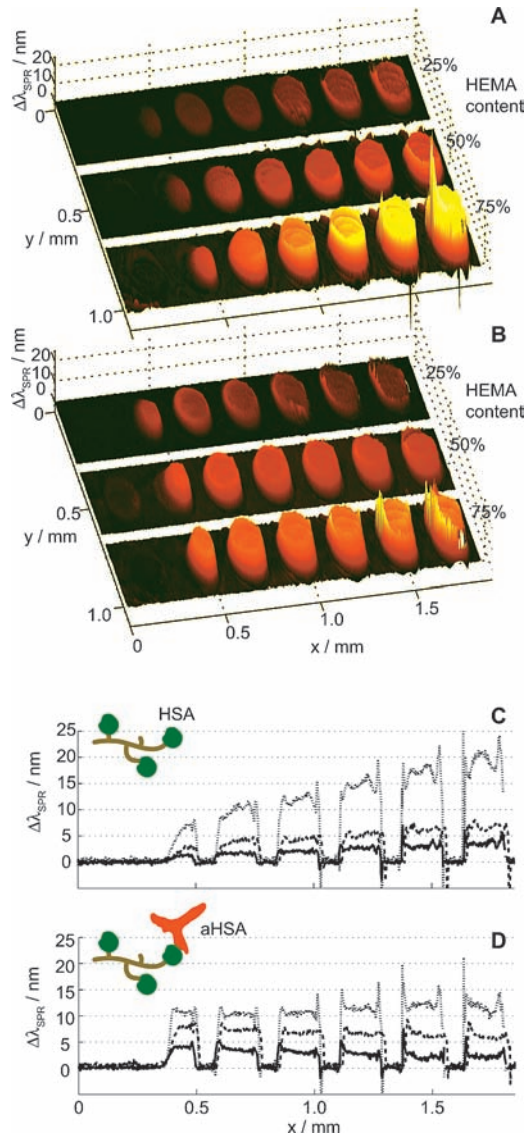

Figure 6. SPR maps of the change in λ_{SPR} upon immobilization of HSA (A) and interaction with aHSA (B). The line profiles in C (HSA) and D (aHSA) show the response of hydrogel spot gradients with different HEMA content: from the top down, 75 (dotted), 50 (dashed), and 25% (solid). No nonspecific binding to the HS-UDA-mPEG in between the hydrogel spots can be observed.

matrix gradients is shown. As can be seen in the line profiles in Figure 6C, the protein loading capacity of the spots increases with increasing HEMA content. As expected, the amount of HSA binding to the matrix is also higher the thicker the spots are. All substrates were activated in the same manner, by flowing of a mixture of EDC/NHS over the surface for five minutes. After immobilization, any remaining anchors were deactivated by flow of ethanolamine for 7 min. The lower immobilization capacity of the matrices rich in $PEG_{10}MA$, seemingly reflects the higher abundance of protein repellent PEG chains. In part, this could also be attributed to a difference in the susceptibility of the hydroxyl end groups of the $PEG_{10}MA$ compared to the HEMA monomers to introduction of carboxyl groups and subsequent EDC/NHS activation, as revealed by recent infrared reflection absorption spectroscopy measurements.[10,11] The iSPR response upon activation of the hydrogel spots is, however, nearly uniform when taking into account the difference in spot thickness and molecular weight of the two monomers (data not shown). The pH dependence of the immobilization was not investigated in this work. However, by using a low pH (4.5 in this case), charge attraction between the negatively charged non activated carboxyl groups in the matrix and positive groups on the protein ligand is likely to aid in immobilization. To control the ligand loading capacity of the hydrogel matrix, it is also necessary to investigate the influence of the contact time during activation, which in the present case was 5 min, and the pH of the coupling buffer on the immobilization level.

In this contribution, we have shown that iSPR can be used to comprehensively visualize and evaluate the binding properties of our hydrogel matrix chip. This is useful when optimizing the performance of hydrogel matrices for future biosensor and microarray applications. The fact that the response of HSA binding increases with the thickness is an indication that this protein is able to penetrate, at least partially, into the hydrogel matrix. The maximum response of $\Delta\lambda_{SPR} \approx 20$ nm corresponds to an effective thickness (if HSA would bind on top of the matrix) of the HSA layer of ~10 nm, which is significantly more than a monolayer. Contrary to the immobilization of HSA, the response after addition of the antibody (aHSA) to the chips does not seem to depend on the hydrogel thickness. As can be seen in the surface map and line profiles of Figure 6C and D, the response of aHSA binding is almost the same to all hydrogel thicknesses. Due to the difference in molecular size of HSA and aHSA, and because aHSA is polyclonal, the change in SPR wavelength upon binding of the antibody is expected to be more than twice that of the ligand response. This is the case only for the thinnest spots. The hydrogel matrix spot gradient with 75% HEMA content, onto which the most HSA could be immobilized, also binds the most aHSA. However, the effective thickness (assuming a homogeneous protein layer on top of the hydrogel) of the aHSA layer is ≤ 5 nm ($\Delta\lambda_{SPR} \approx 10$ nm), which is less than a full monolayer. Further, because the response does not increase with increasing thickness, it appears that all of the ligand is not available for interaction with the analyte. It is very likely that the hydrogel matrix is too dense or cross-linked, in such a way that the larger aHSA (146 kDa) antibody is unable to penetrate as deep as the HSA (66 kDa) protein molecules. The increase in aHSA binding with increasing HEMA content seemingly reflects the level of immobilized HSA. Thus, it seems reasonable to assume that the antibodies bind to HSA present in the outermost portion of the hydrogel, forming an adlayer on top of the matrix, and that there is no discernible difference in diffusion of aHSA within the differently composed matrices. Cross-linking can occur during the grafting process but also during immobilization, due to multipoint attachment of HSA proteins to activated carboxyl groups. This finding is also supported by infrared reflection absorption-measurements that points toward a large degree of size-selectivity of the hydrogel matrix.[11]

CaM−CBD Biointeraction Analysis. To further study the size-selectivity of the hydrogel spot gradient a low molecular weight ligand-analyte system was employed. A commercially available 2.2 kDa calmodulin binding peptide was bound to the hydrogel using amine coupling, and the interaction with calmodulin (17 kDa) was subsequently studied. Based on the findings from the HSA-aHSA study, we opted in this case for a matrix with 75% HEMA. Figure 7A−D show SPR maps and line profiles of the binding of CBD and CaM. As can be seen, there is a clear dependence on spot thickness of the SPR response for both the ligand and analyte. Contrary to the aHSA, the CaM response does not seem to level off as the hydrogel thickness increases. This suggests that the smaller sized CaM is able to penetrate the matrix to a greater extent than the larger

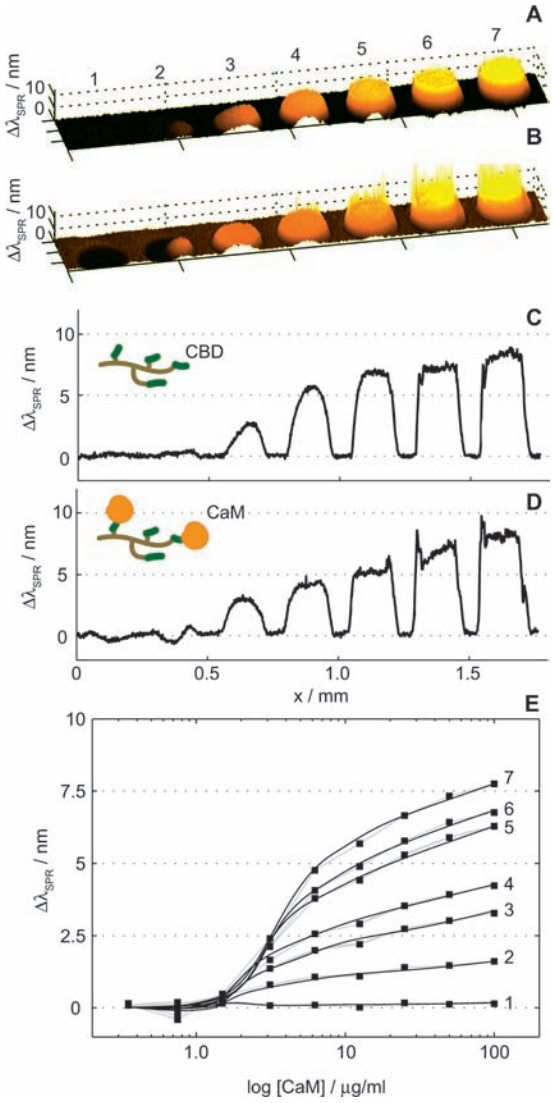

Figure 7. Immobilization of the calmodulin binding domain peptide (CBD) and the subsequent binding of calmodulin (CaM). SPR map showing binding of CBD (A) and 100 μg/mL CaM (B) to a hydrogel spot gradient. Line profiles (C and D) taken across the same row as in A and B. SPR response curves (E) showing the calmodulin concentration dependence for each hydrogel spot (arabic numerals 1−7). The solid lines are included as guides.

sized antibody. Hence, the hydrogel matrix exhibits certain selectivity and seems to be capable of filtering with respect to molecular size, thus acting as a molecular sieve. The response curves in Figure 7E further illustrate this point. Herein, the dependence on the CaM concentration of the SPR response is shown for each spot of the gradient. In quantitative terms, one would expect the response upon binding of CaM to be significantly larger than the CBD response due to the difference in molecular weight. The fact that this is not the case leads us to suggest that all immobilized CBD peptides might not be accessible for the CaM. Another plausible cause for this is that the level of peptide immobilization is so large that saturation is not reached for the CaM concentrations used herein. As can be seen in Figure 7E, the slope of the curve does not level off completely even for the highest concentration. Even so, since the response increases with hydrogel thickness, it can be concluded that the best performance of the PEG_{10}MA/HEMA hydrogel for a small-sized biomolecular system is achieved for the thickest matrix.

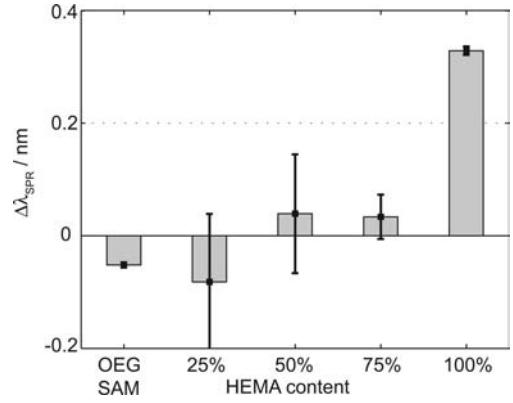

Figure 8. SPR response after deactivation of hydrogel matrix spot gradients with different HEMA content. The reading was made 2 min after a finished injection of 1.4 μM HFib dissolved in HBS-EP, pH 7.4. The confidence bars shows the standard deviation from three spots on the same sample. For reference, the nonspecific binding to the HS-UDA-mPEG SAM is also shown. Only the response to the thickest hydrogel spots of each sample is shown (Note that the response level for 100% HEMA is close to the resolution of the imaging SPR instrument).

Nonspecific Binding During Interaction Analysis. The role of the PEG_{10} chains of the hydrogel matrix is to improve resistance to protein adsorption and inhibit nonspecific binding during the biomolecular interaction analysis. Nonspecific binding to the differently composed hydrogel matrices was investigated by flowing of HFib dissolved in buffer over the surfaces. When using an acidic buffer (sodium acetate pH 4.5) and flowing of HFib at a concentration of 1.4 μM (500 μg/mL) over a carboxylated surface before treatment with EDC/NHS, the SPR wavelength shift due to nonspecifically bound HFib was around 1 nm (data not shown). No significant difference between the differently composed matrices could be observed. The measured response of the nonspecific binding was taken two minutes after the end of the HFib injection. During the injection, however, the hydrogel matrices with a high PEG_{10}MA content showed a lower degree of protein adsorption than the HEMA matrix. The protein resistant PEG chains probably account for most of this effect but it could also be that the HEMA matrix is more porous to the large HFib protein. Figure 8 shows the nonspecific binding of HFib dissolved in HBS-EP buffer at a pH of 7.4 to surfaces that were activated with EDC/NHS and thereafter deactivated with ethanolamine. The response levels are all very low, typically ≤1% of the specific response of aHSA in Figure 6, but the nonspecific binding is slightly higher for the 100% HEMA matrix. The difference between the other matrix compositions is not significant, indicating that a PEG_{10}MA content of 25% is sufficient to eliminate nonspecific binding in this case. For comparison, the iSPR response to the pure OEG-SAM is also included in Figure 8. The nonspecific binding to the OEG-SAM is also very low, proving the usefulness of the SAM as a passive barrier between the spots. The nonspecific binding of HFib did not seem to depend on the thickness of the spots, possibly because of size discrimination of the large-sized protein HFib (M_w = 340 kDa); therefore, the responses given in Figure 8 are taken for the thickest hydrogel spot only, representing an UV graft polymerization time of some 220 s. It should be noted that this exposure time results in fairly equal hydrogel thicknesses (d = 70 nm) for the 25, 50, and 75% HEMA compositions, but that the 100% HEMA hydrogel, which exhibits the highest level of nonspecific binding, is considerably thinner (d = 40 nm).

Conclusions

A hydrogel matrix spot gradient, suitable as a template for evaluating specific as well as nonspecific binding phenomena to protein microarray sensors, was UV-graft copolymerized from a mixture of $PEG_{10}MA$ and HEMA monomers onto OEG-SAM modified gold surfaces. By varying the grafting time laterally, using a photomask and a motorized shutter, rows of spots with thicknesses ranging from 0−70 nm surrounded by inert OEG barriers was grafted on the same chip. The spots exhibited a sloping profile, mainly an effect of diffusion of inhibitors and oxygen from unexposed areas that interfered with the grafting process. The performance of the hydrogel matrix was studied through an in situ biomolecular interaction study of HSA and aHSA using spot gradients of different relative HEMA: $PEG_{10}MA$ compositions. A $PEG_{10}MA$ content of 25% successfully eliminated nonspecific adsorption of HFib to the hydrogel matrix. It was also shown that the loading capacity of HSA to the carboxyl groups introduced in the matrix, increases with increasing HEMA content. Therefore, we conclude that, for practical purposes, a HEMA content of 75% is viable. The regions in between the matrix spots on the chip were covered with a SAM of OEG-thiol. These regions were completely passive to nonspecific binding of the investigated species, HFib, HSA, and aHSA under in situ conditions, providing excellent grid barriers to the active spots.

The permeability of the matrix to large molecules seems to be hampered. This can be disadvantageous as steric constraints may hinder the biospecific interactions. On the other hand, low porosity may aid in reducing nonspecific binding through the exclusion of large biomolecules, and can be an advantage in interaction analysis of small species. The CBD−CaM interaction analysis shows that for small molecular systems a thicker matrix is beneficial. For HSA-aHSA there was no difference in response between spots with different thicknesses, owing to size exclusion of the large antibody. Our hydrogel surface fabrication approach, which allows for thin and thick spots to be created with ease on the same chip, is therefore particularly suitable in array applications where detection of analytes with different sizes is desired.

In all, our approach of using iSPR to evaluate the performance of the hydrogel spot matrix in biosensor applications was proven efficient. The requirement set by the thickness gradient for a large dynamic range could be met using iSPR in spectral interrogation mode. It is furthermore concluded that iSPR is a very useful technique for quick evaluation of the performance of this type of hydrogel matrices and to screen for optimal thickness and composition.

Acknowledgment. This work was supported by the Swedish Research Council (VR), the Foundation for Strategic Research (SSF) through the Biomimetic Materials Science Program and the European Commission through the Integrated Project "HealthCARE by Biosensor Measurements and Networking" (CARE-MAN, NMP4-CT-2006-017333).

References and Notes

(1) Löfås, S.; Johnsson, B. *J. Chem. Soc., Chem. Commun.* **1990**, *21*, 1526–1528.
(2) Ellerby, L. M.; Nishida, C. R.; Nishida, F.; Yamanaka, S. A.; Dunn, B.; Valentine, J. S.; Zink, J. I. *Science* **1992**, *255* (5048), 1113–1115.
(3) Yamanaka, S. A.; Nishida, F.; Ellerby, L. M.; Nishida, C. R.; Dunn, B.; Valentine, J. S.; Zink, J. I. *Chem. Mater.* **1992**, *4* (3), 495–497.
(4) Munoz, E. A.; Yu, H. N.; Hallock, J.; Edens, R. E.; Linhardt, R. J. *Anal. Biochem.* **2005**, *343* (1), 176–178.
(5) Lata, S.; Piehler, J. *Anal. Chem.* **2005**, *77* (4), 1096–1105.
(6) Piehler, J.; Brecht, A.; Valiokas, R.; Liedberg, B.; Gauglitz, G. *Biosens. Bioelectron.* **2000**, *15* (9−10), 473–481.
(7) Huang, N. P.; Voros, J.; De Paul, S. M.; Textor, M.; Spencer, N. D. *Langmuir* **2002**, *18* (1), 220–230.
(8) Masson, J. F.; Battaglia, T. M.; Kim, Y. C.; Prakash, A.; Beaudoin, S.; Booksh, K. S. *Talanta* **2004**, *64* (3), 716–725.
(9) Larsson, A.; Du, C.-X.; Liedberg, B. *Biomacromolecules* **2007**, *8* (11), 3511–3518.
(10) Larsson, A.; Ekblad, T.; Andersson, O.; Liedberg, B. *Biomacromolecules* **2007**, *8*, 287–295.
(11) Larsson, A.; Liedberg, B. *Langmuir* **2007**, *23* (22), 11319–11325.
(12) Zhou, Y.; Andersson, O.; Lindberg, P.; Liedberg, B. *Microchim. Acta* **2004**, *147* (1−2), 21–30.
(13) Zhou, Y.; Andersson, O.; Lindberg, P.; Liedberg, B. *Microchim. Acta* **2004**, *146* (3−4), 193–205.
(14) Valiokas, R.; Klenkar, G.; Tinazli, A.; Tampe, R.; Liedberg, B.; Piehler, J. *ChemBioChem* **2006**, *7* (9), 1325–1329.
(15) Kannan, B.; Castelino, K.; Chen, F. F.; Majumdar, A. *Biosens. Bioelectron.* **2006**, *21* (10), 1960–1967.
(16) Liedberg, B.; Nylander, C.; Lundström, I. *Sens. Actuators* **1983**, *4*, 299–304.
(17) Raether, H. *Surface Plasmons on Smooth and Rough Surfaces and on Gratings*; Springer-Verlag: Berlin-Heidelberg, 1988; Vol. 111.
(18) Kretschmann, E.; Raether, H. *Z. Naturforsch.* **1968**, *A23*, 2135–2136.
(19) Rothenhausler, B.; Knoll, W. *Nature* **1988**, *332* (6165), 615–617.
(20) Stenberg, E.; Persson, B.; Roos, H.; Urbaniczky, C. *J. Colloid Interface Sci.* **1991**, *143* (2), 513–526.
(21) Zhang, L. M.; Uttamchandani, D. *Electron. Lett.* **1988**, *24* (23), 1469–1470.
(22) Yuk, J. S.; Hong, D. G.; Jung, H. I.; Ha, K. S. *Sens. Actuators, B* **2006**, *119* (2), 673–675.
(23) Yuk, J. S.; Kim, H. S.; Jung, J. W.; Jung, S. H.; Lee, S. J.; Kim, W. J.; Han, J. A.; Kim, Y. M.; Ha, K. S. *Biosens. Bioelectron.* **2006**, *21* (8), 1521–1528.
(24) Homola, J. *Sens. Actuators, B* **1997**, *41*, 207–211.
(25) Yuk, J. S.; Jung, J. W.; Jung, S. H.; Han, J. A.; Kim, Y. M.; Ha, K. S. *Biosens. Bioelectron.* **2005**, *20* (11), 2189–2196.
(26) Yuk, J. S.; Yi, S. J.; Lee, H. G.; Lee, H. J.; Kim, Y. M.; Ha, K. S. *Sens. Actuators, B* **2003**, *94* (2), 161–164.
(27) Johansen, K.; Ståhlberg, R.; Liedberg, B. *Meas. Sci. Technol.* **2000**, *11*, 1630–1638.
(28) Hansen, W. N. *J. Opt. Soc. Am.* **1968**, *58* (3), 380–390.
(29) Johansen, K.; Arwin, H.; Lundström, I.; Liedberg, B. *Rev. Sci. Instrum.* **2000**, *71* (9), 3530–3538.

BM801029B